# Performance Comparison of Conventional STATCOM and STATCOM with Energy Storage in a Low Voltage Induction Motor Application

Antti Virtanen
Department of Electrical Energy Engineering
Tampere University of Technology
Tampere, Finland
antti.a.virtanen@tut.fi

Heikki Tuusa
Department of Electrical Energy Engineering
Tampere University of Technology
Tampere, Finland
heikki.tuusa@tut.fi

***Abstract*—This paper presents a performance comparison between a conventional STATCOM and a STATCOM with an integrated energy storage (ESTATCOM), within a low voltage stone crusher application. The systems are compared in terms of supply grid current rating mitigation capabilities, line voltage regulation and voltage flicker compensation characteristics. In addition, the required current ratings for the compensator inverter bridges, as well as the system total energy consumptions are studied. The functionality and power losses of the ESTATCOM have been studied with a small-scale laboratory test setup and the full-scale systems by computer simulations with Matlab Simulink software. According to the research results the ESTATCOM shows best performance within line voltage regulation, voltage flicker compensation, and supply current mitigation properties. In addition the ESTATCOM inverter bridge could be rated significantly smaller than the one of the conventional STATCOM. Load compensation increases the system energy consumptions when the supply grid is strong, but when the supply grid is weak the ESTATCOM consumes slightly less energy than the other studied cases. Overall, load compensation becomes most beneficial within weak supply grids with the STATCOM devices studied.**

## I. INTRODUCTION

Power quality issues such as harmonic distortion, voltage flicker and voltage sags may be compensated with flexible ac transmission system devices (FACTS) such as active filters and static synchronous compensators (STATCOM) [1], [2]. Typically active filters are used for high-order harmonics compensation and STATCOMs for reactive power compensation and point of common coupling (PCC) voltage regulation [1], [2]. The current trend of increasing distributed generation and the concept of smart grid will presumably increase the number of FACTS devices connected to the grid. Local energy storages (ES), such as batteries and supercapacitors (SC), are also seen as an important part of the smart grid, since peaks in production and consumption can be flattened by temporarily storing electrical energy [3]. The above mentioned facts highlight the concept of integrating ES into STATCOMs, which enables the STATCOM to provide also active power support to the grid in addition to the conventional STATCOMs reactive power.

This paper presents a performance comparison between a conventional STATCOM and a STATCOM with integrated energy storage (ESTATCOM) in a low voltage induction motor (IM) application. The systems are compared in terms of supply grid current rating mitigation, line voltage regulation and voltage flicker compensation characteristics. In addition, the required current ratings for the compensator inverter bridges, as well as the system total energy consumptions are studied.

The non-compensated system (NC) consists of a directly grid-coupled IM driving a stone crusher, which is known to cause heavy fluctuation in the power drawn from the grid [4]. Stone crushers are typically used in the mining industry and in rural areas where the strength of the supply grid may be very weak. Thus, the variance of the supply grid strength is also taken into account by studying the systems within three different strength supply grids.

The research has been divided into two parts: experimental tests and computer simulations. The experimental tests include verification of the ESTATCOM operation in practice with a small-scale laboratory test setup, and power loss measurements of the system components during operation. The computer simulations consist of full-scale system modeling and simulation with the power loss models developed on the basis of the small-scale laboratory measurements.

Section II presents the compensation systems studied and their control principles. Section III presents the ESTATCOM laboratory test setup and its simulation model. Section IV presents the full-scale system simulation models and the analysis of the simulation results. Finally, the conclusions are drawn in Section V.

## II. THE COMPENSATION SYSTEMS

### A. STATCOM with Integrated Energy Storage (ESTATCOM)

Fig. 1 presents the main circuit and control system of the ESTATCOM. It consists of a shunt-connected voltage source inverter with an SC bank connected to the system dc link via a bidirectional DC-DC converter. An LCL-filter is included to damp the switching frequency ripple of the inverter current $\underline{i}_{\text{inv}}$. The aim of the control is to draw steady average active power from the grid and fully compensate the reactive power of the load. During system operation the SC is discharged when the instantaneous active power of the load is greater than the average, and charged when the active power is lower than the average.

The control system can basically be divided into three parts: one consisting of the inverter side to control $\underline{i}_{\text{inv}}$, and the second to regulate the dc link voltage $u_{\text{dc}}$ with the combination of the DC-DC converter and the SC. The third control branch is used to keep the SC voltage $u_{\text{SC}}$ within its desired operating range under long-term operation.

The inverter control system is based on the *p-q* theory implemented in a stationary (α,β) reference frame. First the instantaneous active and imaginary powers ($p_{\text{l}}$, $q_{\text{l}}$) of the load are calculated on the basis of load current $\underline{i}_{\text{l}}$ and PCC voltage $\underline{u}_{\text{PCC}}$ measurements in the PQ-block [1], [4]

$$p_{\text{l}} = \frac{3}{2}(u_{\text{PCC}\alpha} i_{\text{l}\alpha} + u_{\text{PCC}\beta} i_{\text{l}\beta})$$
$$q_{\text{l}} = \frac{3}{2}(u_{\text{PCC}\beta} i_{\text{l}\alpha} - u_{\text{PCC}\alpha} i_{\text{l}\beta}). \quad (1)$$

The active power reference $p_{\text{f,ref}}$ is found by inverse low-pass filtering $p_{\text{l}}$ (1st order LPF with time constant $\tau = 2.5$ s) and adding the SC voltage controller output $p_{\text{f0}}$. The imaginary power reference $q_{\text{f,ref}}$ is found by inverting $q_{\text{l}}$, since the aim is to fully compensate the load imaginary power. After these operations the current reference $\underline{i}_{\text{inv,ref}}$ is calculated in the G($p$,$q$,$\underline{u}_{\text{PCC}}$)-block as follows [1], [4]:

$$i_{\text{inv}\alpha,\text{ref}} = \frac{2}{3}\left(\frac{p_{\text{f,ref}} u_{\text{PCC}\alpha} + q_{\text{f,ref}} u_{\text{PCC}\beta}}{u_{\text{PCC}\alpha}^{\ 2} + u_{\text{PCC}\beta}^{\ 2}}\right)$$
$$i_{\text{inv}\beta,\text{ref}} = \frac{2}{3}\left(\frac{p_{\text{f,ref}} u_{\text{PCC}\beta} - q_{\text{f,ref}} u_{\text{PCC}\alpha}}{u_{\text{PCC}\alpha}^{\ 2} + u_{\text{PCC}\beta}^{\ 2}}\right). \quad (2)$$

Finally the current control-loop produces the LCL-filter voltage reference $\underline{u}_{\text{LCL,ref}}$, and the inverter voltage reference $\underline{u}_{\text{inv,ref}}$ is obtained by subtracting $\underline{u}_{\text{LCL,ref}}$ from the measured $\underline{u}_{\text{PCC}}$.

The DC-DC converter control system is based on feedback control of the measured $u_{\text{dc}}$. The objective is to keep $u_{\text{dc}}$ around its reference value $u_{\text{dc,ref}}$.

### B. Conventional STATCOM

The main circuit and control system of the conventional STATCOM is presented in Fig. 2. The difference with the ESTATCOM is that the system includes a PCC voltage controller, which outputs an imaginary power reference $q_{\text{PCC,ref}}$. With positive $q_{\text{PCC,ref}}$ the system injects imaginary power to the grid increasing $\underline{u}_{\text{PCC}}$, and with negative $q_{\text{PCC,ref}}$ the system draws imaginary power from the grid and $\underline{u}_{\text{PCC}}$ decreases [5], [6]. The time constant of the PCC voltage controller LPF is $\tau = 2.5$ s and the time constant of the LPF for $p_{\text{l}}$ filtering is $\tau = 2.27$ ms in order to compensate the possible load harmonics.

## III. ESTATCOM LABORATORY TEST SETUP AND SIMULATION MODEL

This section presents the structure of the ESTATCOM laboratory test setup. In addition, the development of the simulation model including power loss models for the system components is presented and the experimental results are compared with the simulation results.

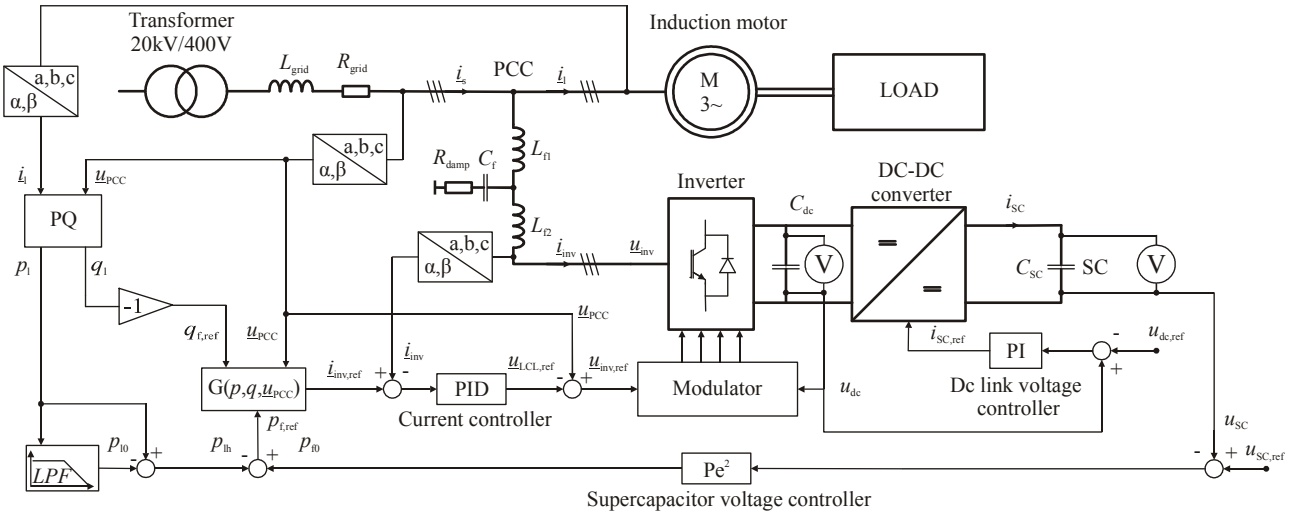


Figure 1. ESTATCOM main circuit and control system.

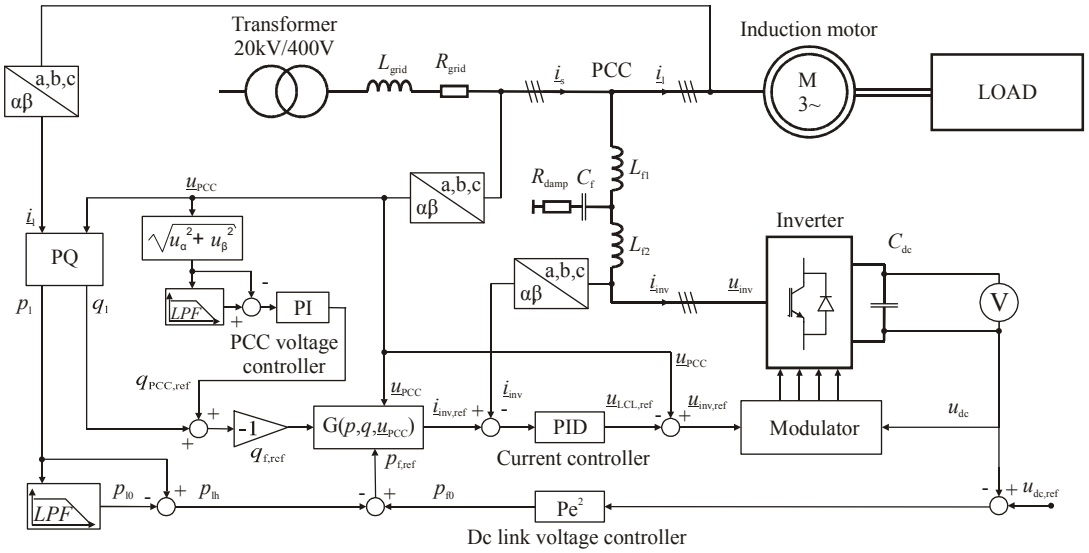


Figure 2. STATCOM main circuit and control system.

### A. *Test Setup Structure and Components*

The control system of the ESTATCOM laboratory test setup was similar to the one presented in Fig. 1. The structure of the setup and the measurement devices used are presented in Fig. 3, and the system component parameters in Table I. A photograph of the test-setup is presented in Fig. 4.

The nominal power of the IM was 11 kW, and a 62 kW separately exited DC machine fed by a three-phase four-quadrant thyristor rectifier was used to emulate the stone crusher load. The supply grid impedance was composed of an inductor of $L_{grid}$ = 1.7 mH and $R_{grid}$ = 13 mΩ, in order to artificially weaken the supply grid. The ESTATCOM inverter was a three-phase two-level inverter with rated power of 18 kVA. It was built by modifying a commercial frequency converter into an active power filter [7]. The inverter IGBT-switches were of type SKM 75GB176D. The DC-DC converter was a commercial bidirectional converter of type Msc 200DCDC750 with rated power of 90 kW. The supercapacitor was a Maxwell BMOD0063 P125 module with a nominal capacitance of 63 F and nominal voltage of 125 V.

A Motorola MPC555 microcontroller was used to implement the inverter control. The dc link and SC voltage control systems, as well as supplying the load torque reference for the thyristor rectifier, were carried out with dSPACE ds1103 real-time simulation platform. The measurements were carried out with the following instruments. For measuring $i_{SC}$ and $i_{dc}$ Tektronics TCP303 current probes together with TCPA300 amplifiers were used, and $u_{SC}$ and $u_{dc}$ were measured with Tektronics P5200 high voltage differential probes. For the three-phase ac quantities three analog universal power meters (UPM), each consisting of LEM LA 50-P current transducers and differential voltage measurement units for each phase, were used. The load torque $T_l$ and rotational speed $n_l$ were measured with a HBM T30FN torque transducer and a HBM DA 3418 amplifier.

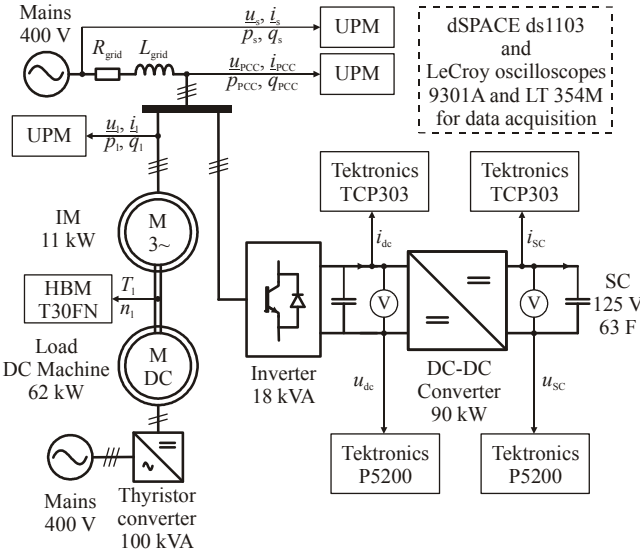


Figure 3. Structure and measurement devices of the ESTATCOM laboratory test setup.

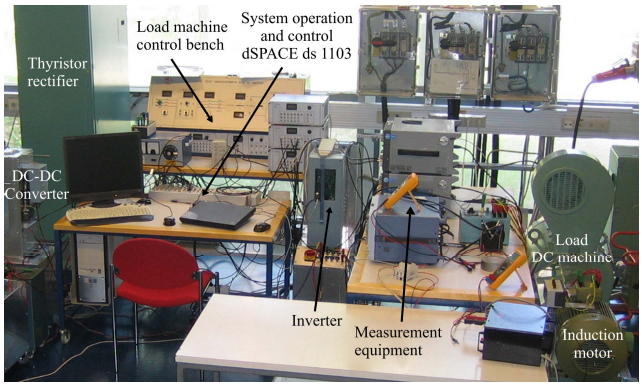


Figure 4. Photograph of ESTATCOM laboratory test setup.

TABLE I COMPONENTS AND SYSTEM PARAMETERS OF ESTATCOM LABORATORY TEST SETUP

| | |
|---|---|
| **Induction Motor** | |
| Nominal shaft power $P_N$ | 11 kW |
| Nominal voltage $U_N$ | 380 V |
| Nominal current $I_N$ | 23 A |
| **Supply Grid Impedance** | |
| Grid inductance | $L_{grid}$ = 1.7 mH (0.051 pu) |
| Grid resistance | $R_{grid}$ = 13 mΩ (0.0012 pu) |
| **ESTATCOM (IGBTs: SKM 75GB176D)** | |
| Rated power $S_N$ | 18 kVA |
| Switching frequency $f_s$ | 10 kHz |
| LCL filter inductor $L_{f1}$ | 0.6 mH (0.022 pu) |
| ESR of $L_{f1}$ | 20 mΩ (0.002 pu) |
| LCL filter inductor $L_{f2}$ | 6 mH (0.22 pu) |
| ESR of $L_{f2}$ | 100 mΩ (0.01 pu) |
| LCL filter capacitor $C_f$ | 30 µF (0.08 pu) |
| Damping resistor $R_{damp}$ | 4.5 Ω (0.53 pu) |
| Dc link capacitance $C_{dc}$ | 3.35 mF (8.96 pu) |
| Dc link voltage reference $u_{dc,ref}$ | 730 V |
| **DC-DC Converter (Msc 200DCDC750)** | |
| Rated power | 90 kW |
| Maximum continuous current | 120 A |
| Maximum peak current | 200 A, 1 min every 10 min |
| **Supercapacitor Module (Maxwell BMOD0063 P125)** | |
| SC nominal capacitance $C_{SC}$ | 63 F (168450 pu) |
| SC nominal voltage $u_{SC}$ | 125 V |
| SC voltage reference $u_{SC,ref}$ | 115 V |

### B. *Laboratory Test Setup Simulation Model for Component Power Loss Modeling*

A simulation model of the ESTATCOM laboratory test setup was developed simultaneously with the experimental tests. The main objective was to accurately model the power losses of the system components in order to use the power loss models in the full-scale system simulations. The following power losses were taken into account in the simulations: 1) inverter conduction and switching losses, 2) LCL-filter iron and copper losses, and 3) DC-DC converter losses and SC losses. The parameters of the power loss models are presented in Table II.

#### 1) *Inverter Conduction and Switching Losses*

In the calculation of both the inverter conduction and switching losses it is assumed that the inverter operates with sinusoidal currents, and that the calculated losses are achieved as an average over the 50 Hz fundamental period. The average conduction losses for one active switching device $P_{C-SW}$ and one antiparallel diode $P_{C-D}$ in a three-phase two-level inverter, can be calculated from [8], [9]

$$P_{C-SW} = \frac{1}{2}\hat{i}_{inv}V_t\left(\frac{1}{\pi}+\frac{M}{4}\cos\varphi\right)+\hat{i}_{inv}^2 R_{CE}\left(\frac{\sqrt{3}}{8\sqrt{\pi}}+\frac{M}{3\pi}\cos\varphi\right) \quad (3)$$

$$P_{C-D} = \frac{1}{2}\hat{i}_{inv}V_f\left(\frac{1}{\pi}-\frac{M}{4}\cos\varphi\right)+\hat{i}_{inv}^2 R_{AK}\left(\frac{\sqrt{3}}{8\sqrt{\pi}}-\frac{M}{3\pi}\cos\varphi\right), \quad (4)$$

TABLE II PARAMETERS OF ESTATCOM LABORATORY TEST SETUP POWER LOSS MODELS

| | |
|---|---|
| IGBT zero-current voltage drop $V_t$ | 0.9 V |
| Diode zero-current voltage drop $V_f$ | 0.9 V |
| IGBT on-state resistance $R_{CE}$ | 31 mΩ |
| Diode on-state resistance $R_{AK}$ | 18 mΩ |
| IGBT loss energy determination voltage $u_{CC}$ | 1200 V |
| Inverter ventilation & control losses $P_{vent}$ | 75 W |
| LCL-filter iron losses $P_{loss,fs,LCL}$ | 150 W |
| DC-DC converter minimum losses $P_{loss,min,DCDC}$ | 300 W |
| SC one way efficiency $\eta_{SC}$ | 0.985 |

where $\hat{i}_{inv}$ is the peak-value of the sinusoidal inverter current, $V_t$ and $V_f$ the voltage drops at zero-current condition for the IGBT and diode, $R_{CE}$ and $R_{AK}$ the resistive elements of the IGBTs and diodes, cos $\varphi$ the displacement power factor, and $M$ is the modulation index calculated from

$$M = \frac{\left|\underline{u}_{inv,ref}\right|}{u_{dc}/2}. \quad (5)$$

Parameters $V_t$, $V_f$, $R_{CE}$, and $R_{AK}$ can be obtained from manufacturer's datasheets.

The inverter average switching loss model consists of IGBT turn-on and turn-off losses $P_{ON/OFF-SW}$, and diode reverse recovery losses $P_{RR-D}$, respectively. These are calculated from [10]

$$P_{ON/OFF-SW} = \frac{1}{\pi}\cdot f_s \cdot \frac{u_{dc}}{u_{CC}}\cdot\left[E_{ON}(\hat{i}_{inv})+E_{OFF}(\hat{i}_{inv})\right] \quad (6)$$

$$P_{RR} = \frac{1}{\pi}\cdot f_s \cdot \frac{u_{dc}}{u_{CC}}\cdot E_{RR}(\hat{i}_{inv}), \quad (7)$$

as a function of the switching frequency $f_s$ for one active switching device and one antiparallel diode. In (6) and (7) $E_{ON}$, $E_{OFF}$ and $E_{RR}$ are the respective turn-on, turn-off and reverse recovery loss energies as a function of the inverter current, and $u_{CC}$ is the collector-emitter supply voltage used in determination of the loss energies. These parameters can all be obtained from the manufacturer's datasheet.

Finally the total power losses for the six inverter bridge IGBTs and antiparallel diodes can be calculated from

$$P_{LOSS-TOT} = 6\cdot(P_{C-SW}+P_{C-D}+P_{ON/OFF-SW}+P_{RR})+P_{vent}, \quad (8)$$

where $P_{vent}$ is an additional power loss of 75 W of the inverter ventilation fan and control electronics.

#### 2) *LCL-filter Power Losses*

In the modeling of the LCL-filter power losses the copper and iron losses of the filter inductors were taken into account. The copper losses were modeled with appropriate equivalent series resistances (ESR) for inductances $L_{f1}$ and $L_{f2}$. The iron losses caused by the switching frequency ripple of the compensator current were approximated as constant $P_{loss,fs,LCL}$ = 150 W by comparing the simulation results with the measurements.

*3) DC-DC Converter and SC Power Losses*

The power losses for the DC-DC converter were modeled with efficiency maps for the charge and discharge operations, presented respectively in Fig. 5. The maps were obtained by charging and discharging the SC module with currents of 5–120 A, and the efficiency is found as a function of the SC current and the conversion ratio $u_{SC}/u_{dc}$. The minimum power losses of the DC-DC converter were limited to $P_{loss,min,DCDC} = 300$ W in order to cover the losses due to the ventilation and control electronics and due to slight inaccuracies in the maps during low current operation.

The power losses of the SC were modeled with a fixed one-way efficiency of $\eta_{SC} = 0.985$, on the basis of measurements for a Maxwell BMOD0063 P125 module presented in [11].

## C. Measurement and Simulation Results

The measurement results of the ESTATCOM laboratory test setup and the NC system, as well as the respective simulation results during a 60 s load cycle are presented in Figs. 6a–i. In the figures the ESTATCOM measured waveforms are presented in blue, ESTATCOM simulations in red, and NC measurements in black.

Figs. 6a,b present the supply transformer active- and imaginary powers for the systems studied. With the ESTATCOM the active power becomes smoother than with the NC, and steady average power is drawn from the grid. The imaginary power becomes also compensated to zero as anticipated in Section II. Fig. 6c presents the system PCC voltages. During the load cycle $u_{PCC}$ decreases because of the voltage drop over the supply grid impedance. The ESTATCOM is still able to maintain higher and more leveled $u_{PCC}$ than the NC, due to the compensated active- and imaginary powers. Figs. 6d–f present the ESTATCOM dc link voltage, SC current and SC voltage, respectively. The $u_{dc}$ control system keeps $u_{dc}$ around $u_{dc,ref}$, by discharging the SC when the load active power is higher than the average, and by charging the SC when the active power is lower than the average. During long-term operation $u_{SC}$ settles into a voltage value in which the system losses become compensated by the SC voltage controller output $p_{f0}$.

Figs. 6g–h present the measured ESTATCOM total power losses, combined losses of the inverter and LCL-filter, and DC-DC converter losses compared against the respective simulated power losses. The measured and simulated average power losses $P_{loss,avg}$ of the ESTATCOM components during the measurement period are presented in Table III. Despite some inaccuracy between the measured and simulated power losses of the inverter and LCL-filter during the idle period at the beginning and end of the measurement period, the power loss models give a reasonable approximation for the system losses, and can be used in full-scale system modeling.

# IV. Full-Scale System Simulations

## A. Simulated Systems

The simulation models of the ESTATCOM and the NC system developed in Section III were scaled up to match the power levels of the full-scale 250 kW systems. In addition, a simulation model of the conventional STATCOM of Fig. 2 was developed. The parameters of the full-scale systems are presented in Table IV.

The nominal power of the full-scale system IM was 250 kW, and the rated powers of both ESTATCOM and conventional STATCOM inverters were 300 kVA. The per unit values of the LCL-filter passive elements were designed to match those of the ESTATCOM laboratory test setup. The type of the IGBT-modules used in the inverter bridge power loss model was SKM 900GA12E4 and the losses $P_{vent}$ as well as $P_{loss,fs,LCL}$ were multiplied by a factor of 300/18, according to the ratio of the laboratory test setup and full-scale system rated powers. The DC-DC converter power losses were modeled with the efficiency maps presented in Fig. 7, and $P_{loss,min,DCDC}$ was approximated to correspond to three Msc 200DCDC750 converters. The SC bank was composed of two parallel units, both comprising of a series connection of five Maxwell BMOD0063 P125 SC modules.

The systems were simulated in supply grids of three different strengths: strong grid, medium grid, and weak grid. The strong grid consisted of a 500 kVA transformer and an AMMK 3×2×300 cable of 200 m, the medium grid of a 500 kVA transformer and an AMMK 3×2×300 cable of 500 m, and the weak grid of a 500 kVA transformer and an AMMK 3×2×300 cable of 1000 m, respectively. The per unit inductance of the strong grid matched the grid inductance of the laboratory test setup.

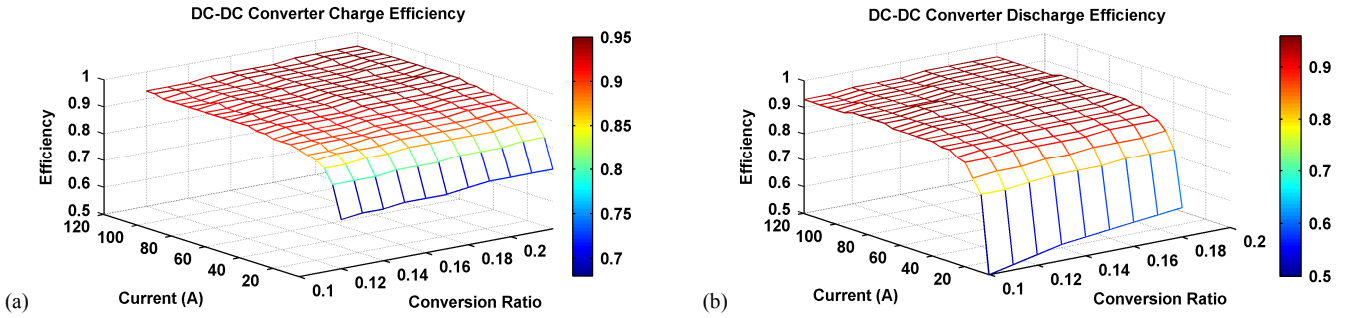


Figure 5. DC-DC converter efficiency maps for (a) charge efficiency, (b) discharge efficiency.

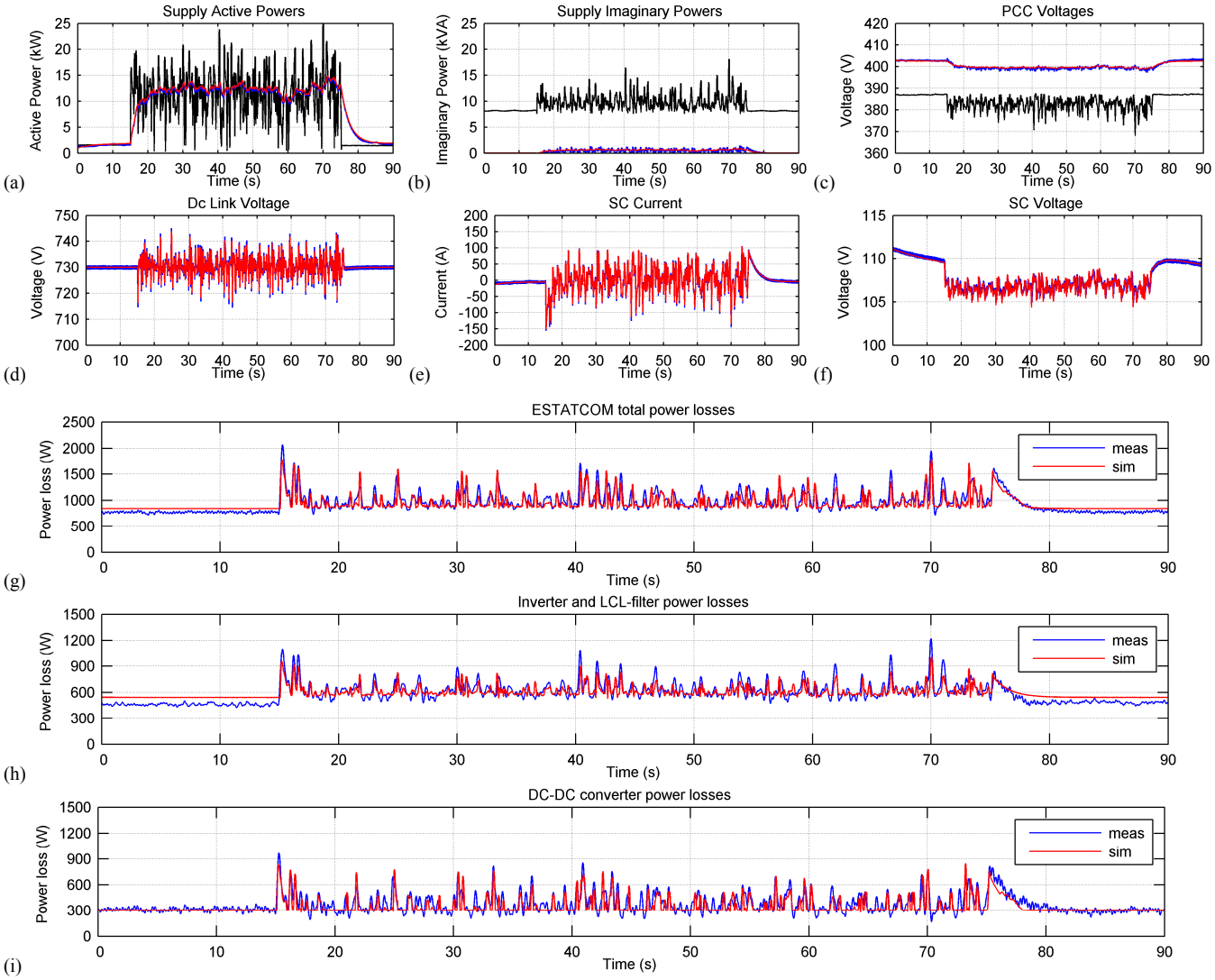


Figure 6. ESTATCOM test setup measurement results. (a) Supply active powers, (b) supply imaginary powers, (c) PCC voltages $u_{PCC,rms}$, (d) Dc link voltage $u_{DC}$, (e) SC current $i_{SC}$, (f) SC voltage $u_{SC}$, (g) ESTATCOM total power losses, (h) inverter and LCL-filter combined power losses, (i) DC-DC converter power losses. ESTATCOM measured (blue), ESTATCOM simulated (red), NC measured (black).

TABLE III MEASURED AND SIMULATED AVERAGE POWER LOSSES OF ESTATCOM LABORATORY TEST SETUP

| System | $P_{loss,avg}$ | |
|---|---|---|
| | Measurement | Simulation |
| DC-DC converter | 370 W | 342 W |
| Inverter + LCL-filter | 590 W | 599 W |
| Total | 960 W | 941 W |

## B. *Simulation Results*

The system performances were analyzed in the following categories:

1) Supply transformer and cable current ratings

2) PCC voltage regulation and system flicker indices

3) Compensator current ratings

4) Total energy consumption

Figs. 8a–f present the simulation results during a 60 s stone crusher load cycle. In the figures the ESTATCOM waveforms are presented in red, the conventional STATCOM in green, and the NC system in blue. A summary of the results is presented in Table V.

### *1) Supply Transformer and Cable Current Ratings*

Fig. 8a presents the supply phase-a currents $I_{s,rms}$ for the studied systems, in the medium grid. The ESTATCOM effectively smoothes the $I_{s,rms}$ waveforms in comparison with the other systems. The results of Table V predict that in the weak grid the rated current of the supply transformer and cables could be approximately 20 % lower with the ESTATCOM, and 10 % lower with the conventional STATCOM than with the NC system, depending of the grid strength.

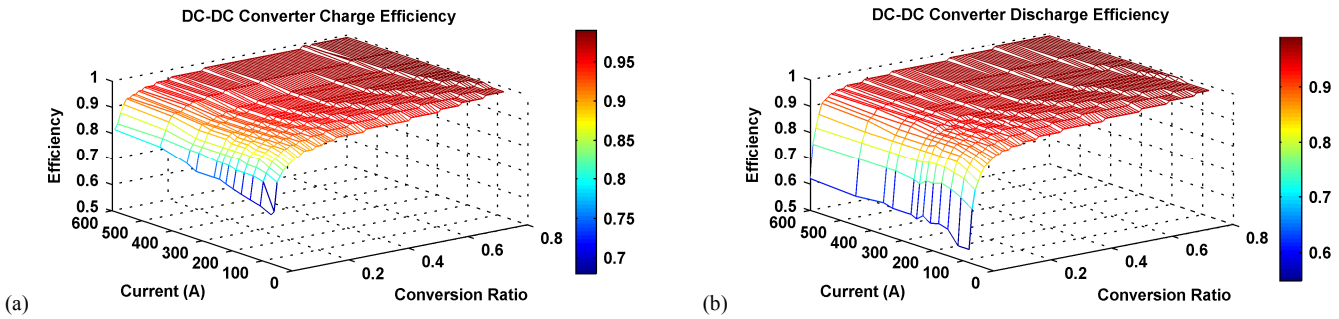


(a) (b)

Figure 7. Efficiency maps of full-scale ESTATCOM DC-DC converter. (a) Charge efficiency, (b) discharge efficiency.

*2) PCC Voltage Regulation and System Flicker Indices*

Fig. 8b presents the $u_{PCC,rms}$ in the medium grid for the studied systems, and Table V the $u_{PCC}$ minimum values and percentual voltage drops of $U_N$ (400 V) respectively. Both compensated systems are able to maintain the $u_{PCC}$ drop at an acceptable level below 15 %, due to power compensation and the $u_{PCC}$ control. The maximum voltage drop of the NC system in the weak grid is 31 %, which is significantly higher than the voltage drops of the compensated systems.

The voltage flicker indices $P_{st}$ of the PCC and supply transformer voltages were analyzed with a flicker meter simulation model implemented in line with the standard IEC-61000-4-15 [12]. With the ESTATCOM all of the cases studied produce $P_{st}$ values below the threshold level for irritating voltage flicker of 1 pu (Table V). With the conventional STATCOM the flicker levels are acceptable in the strong grid, but in the medium- and weak grids the PCC voltage $P_{st}$ values exceed the threshold value. With the NC system the $P_{st}$ threshold level is exceeded in all cases studied, thus load compensation significantly improves the voltage quality.

*3) Compensator Current Ratings*

Fig. 8c presents the currents $I_{inv,rms}$ of the both compensator inverters in the medium grid. The current of the conventional STATCOM has clearly higher peak values than the current of the ESTATCOM. The peak values of the currents determine the current ratings for the IGBT switches of the compensator inverter bridges. It can be observed from Table V that in the case of the strong grid IGBTs with approximately the same rated current could be used in both systems. However, in the medium grid the ESTATCOM IGBTs could be downsized to about 75 %, and in the weak grid to about 63 % compared to the conventional STATCOM IGBTs.

*4) Total Energy Consumption*

Figs. 8d–f present a comparison of the systems' energy consumption as a function of the grid strength. The energy consumptions were calculated assuming that the systems would be in the steady-state mode of the time period of 40–75 s for one hour. In the case of the strong grid the total energy consumption of the ESTATCOM and conventional STATCOM becomes higher than with the NC system, because of the power losses in the compensator power electronics and passive elements. However, in weaker grids the compensator losses become less dominant in proportion to the increasing grid losses. The grid losses increase the most with the NC system, and in the weak grid the total energy consumption with the ESTATCOM becomes approximately one percentage unit lower than with the NC system.

TABLE IV SYSTEM PARAMETERS AND COMPONENTS OF SIMULATED FULL-SCALE SYSTEMS

| | | |
|---|---|---|
| **Induction Motor** | | |
| Nominal shaft power $P_N$ | 250 kW | |
| Nominal voltage $U_N$ | 400 V | |
| Nominal current $I_N$ | 450 A | |
| **Supply Grid Definitions** | | |
| Strong grid (200 m cable) | $L_{grid}$ = 81 µH | (0.050 pu) |
| | $R_{grid}$ = 15 mΩ | (0.029 pu) |
| Medium grid (500 m cable) | $L_{grid}$ = 131 µH | (0.081 pu) |
| | $R_{grid}$ = 33 mΩ | (0.065 pu) |
| Weak grid (1000 m cable) | $L_{grid}$ = 215 µH | (0.132 pu) |
| | $R_{grid}$ = 62 mΩ | (0.122 pu) |
| **ESTATCOM & STATCOM** | | |
| Rated power $S_N$ | 300 kVA | |
| Switching frequency $f_s$ | 10 kHz | |
| LCL filter inductor $L_{f1}$ | 37 µH | (0.022 pu) |
| ESR of $L_{f1}$ | 1 mΩ | (0.002 pu) |
| LCL filter inductor $L_{f2}$ | 370 µH | (0.22 pu) |
| ESR of $L_{f2}$ | 5 mΩ | (0.01 pu) |
| LCL filter capacitor $C_f$ | 130 µF | (0.022 pu) |
| Damping resistor $R_{damp}$ | 0.28 Ω | (0.53 pu) |
| Dc link capacitance $C_{dc}$ | 53.8 mF | (8.96 pu) |
| Dc voltage reference $u_{dc,ref}$ | 800 V | |
| **Inverter Bridge Power Loss Model (SKM 900GA12E4)** | | |
| IGBT zero-current voltage drop $V_t$ | 0.7 V | |
| Diode zero-current voltage drop $V_f$ | 0.9 V | |
| IGBT on-state resistance $R_{CE}$ | 1.7 mΩ | |
| Diode on-state resistance $R_{AK}$ | 1.6 mΩ | |
| IGBT energy determination voltage $u_{CC}$ | 600 V | |
| **Other losses** | | |
| Inverter ventilation & control losses $P_{vent}$ | 1250 W | |
| LCL-filter iron losses $P_{loss,fs,LCL}$ | 2500 W | |
| DC-DC converter min losses $P_{loss,min,DCDC}$ | 900 W | |
| **Supercapacitor Bank** | | |
| SC capacitance $C_{SC}$ | 25.2 F | (4200 pu) |
| SC nominal & reference voltage $u_{SC,ref}$ | 625 V | |
| SC one way efficiency $\eta_{SC}$ | 0.985 | |

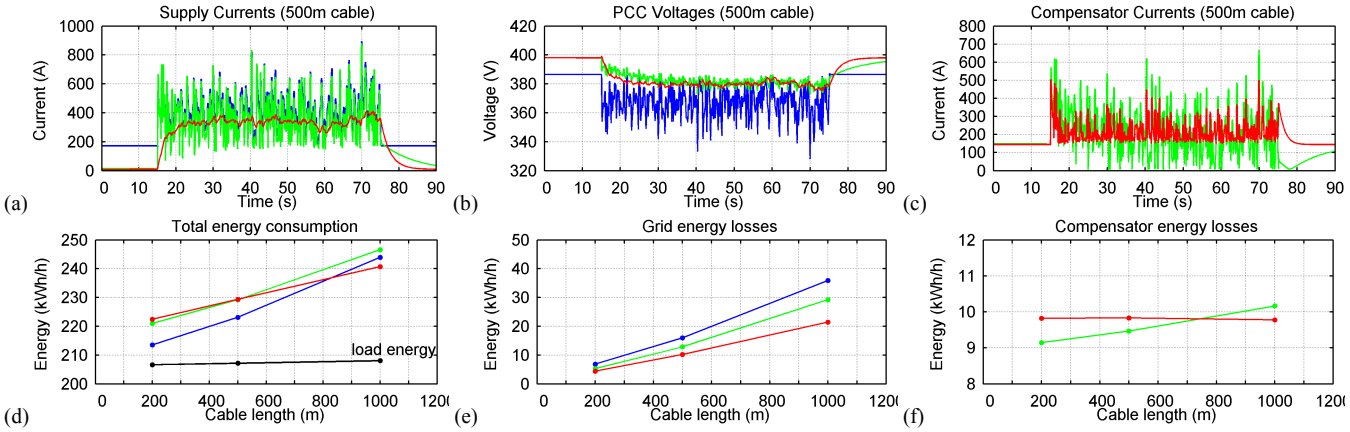


Figure 8. Full-scale system simulation results. (a) Supply currents $i_{s,rms}$, (b) PCC voltages $u_{PCC,rms}$, (c) compensator currents $i_{f,rms}$, (d) total energy consumptions, (e) grid energy losses, and (f) compensator energy losses. ESTATCOM (red), STATCOM (green), NC (blue).

## V. CONCLUSIONS

A performance comparison was presented between the ESTATCOM, conventional STATCOM and the NC system within a stone crusher application. First the functionality of the ESTATCOM was verified with a small-scale 11 kW laboratory test setup and the power losses of the system components were measured. Second, simulation models for modeling the power losses in the ESTATCOM inverter bridge, LCL-filter, DC-DC converter and SC were developed on the basis of the laboratory measurements. Finally, the small-scale simulation models were scaled up to match the power level of a full-scale 250 kW process, and the systems were simulated in three different strength supply grids.

The system performances were analyzed on the basis of the supply grid current ratings, line voltage regulation capabilities, voltage flicker indices, compensator current ratings, and the total energy consumptions. The best performance in line voltage regulation, flicker reduction, and supply grid current mitigation were achieved with the ESTATCOM. In addition the ESTATCOM inverter bridge could be rated significantly smaller than that of the conventional STATCOMs, especially in the weak grid. Load compensation increases the system energy consumptions in the stronger supplies due to power losses in the compensator components. However, in the weak grid the ESTATCOM consumes slightly less energy than the other studied cases. Overall, load compensation becomes most beneficial in the weak supply grid with the STATCOM devices studied.

TABLE V PERFORMANCE COMPARISON OF FULL-SCALE SYSTEMS

| **Supply Current (Arms / % of NC)** | | | |
|---|---|---|---|
| **Case** | **ESTATCOM** | **STATCOM** | **NC** |
| Strong grid | 323 / 80.5 | 354 / 88.3 | 401 / 100 |
| Medium grid | 334 / 80.0 | 374 / 89.7 | 417 / 100 |
| Weak grid | 352 / 77.4 | 410 / 90.1 | 455 / 100 |
| **Minimum PCC Voltage (Vrms / % drop of $U_N$)** | | | |
| Strong grid | 388 / 3 | 386 / 3.5 | 364 / 9.0 |
| Medium grid | 375 / 6.3 | 372 / 7.0 | 328 / 18.0 |
| Weak grid | 351 / 12.3 | 342 / 14.5 | 275 / 31.3 |
| **Voltage flicker indices $P_{st}$ (Supply / PCC)** | | | |
| Strong grid | 0.04 / 0.13 | 0.38 / 0.84 | 1.01 / 3.08 |
| Medium grid | 0.11 / 0.41 | 0.73 / 1.73 | 1.11 / 6.6 |
| Weak grid | 0.11 / 0.79 | 0.92 / 3.58 | 1.26 / 13.58 |
| **Compensator Peak Currents (Arms / % of STATCOM)** | | | |
| Strong grid | 502 / 101.0 | 497 / 100 | - |
| Medium grid | 505 / 75.6 | 668 / 100 | - |
| Weak grid | 506 / 63.3 | 799 / 100 | - |
| **Total Energy Consumption (kWh/h / % of NC)** | | | |
| Strong grid | 222 / 103.7 | 221 / 103.3 | 214 / 100 |
| Medium grid | 229 / 102.7 | 229 / 102.7 | 223 / 100 |
| Weak grid | 241 / 98.7 | 247 / 101.2 | 244 / 100 |

## REFERENCES


[1] H. Akagi, E. H. Watanabe, M. Aredes, Instantaneous power theory and applications to power conditioning, John Wiley & Sons, USA 2007, 379 p.

[2] N. Hingorani, L. Gyugyi, Understanding FACTS, John Wiley & Sons, USA, 2000, 432 p.

[3] M. Bollen, The smart grid: adapting the power system to new challenges, Morgan & Claypool, USA, 2011, 164 p.

[4] A. Virtanen, H. Tuusa, "Power compensator for high power fluctuating loads with a supercapacitor bank energy storage", in proc. IEEE PeCon, 2008, pp. 977-982.

[5] P. S. Sensarma, K.R. Padiyar, V. Ramanarayanan, "Analysis and performance evaluation of a distribution STATCOM for compensating voltage fluctuations", IEEE Trans. Power Delivery, vol. 16, no. 2, April 2001, pp. 259–264.

[6] M. Bongiorno, J. Svensson, "Voltage dip mitigation using shunt-connected voltage source converter", IEEE Trans. Power Electron., vol 22, no 5, Sept. 2007, pp. 1867–1874.

[7] P. Parkatti, M. Routimo, H.Tuusa, "Modification of a commercial frequency converter to an active power filter in 690 V power system", in proc. PCIM Europe, 2007, 6 p.

[8] J. S. Lai, R. W. Young, J. W. McKeever, "Efficiency consideration of DC link soft switching inverters for motor drive applications", in proc. IEEE PESC, 1994, vol. 2, pp.1003-1010.

[9] L. M. Tolbert, F. Z. Peng, T. G. Habetler, "Multilevel converters for large electric drives", IEEE Trans. Ind. Appl., vol. 35, no. 1, Jan/Feb, 1999, pp. 36-44.

[10] U.Nicolai, T.Reimann, J.Petzhold, J. Lutz, P.Martin, SEMIKRON Application Manual, ISLE, Germany, 1998, 270 p.

[11] A. Virtanen, H. Haapala, S. Hännikäinen, T. Muhonen, H. Tuusa, "Calorimetric efficiency measurements of supercapacitors and lithium-ion batteries", in proc. APEC, 2011, pp. 1367-1373.

[12] IEC-61000-4-15, Testing and measurement techniques – Flickermeter – Functional and design specifications, 2003, 47 p.